Photonic Crystal VCSELs: Detailed Comparison of Experimental and Theoretical Spectral Characteristics

Tomasz Czyszanowski, Maciej Dems, Robert P. Sarzała, Krassimir Panajotov, and Kent D. Choquette, *Fellow, IEEE*

***Abstract*—We present a detailed comparison of experimental and simulated optical spectra obtained from a 980-nm photonic-crystal (PhC) VCSEL. We demonstrate good qualitative agreement of the experimental spectra with the calculated emitted wavelengths for number of VCSEL structures with different PhC designs. We show the statistical analysis which reveals that strong confinement introduced by the photonic crystal contributes to the conformity between experiment and theory. For shallow etching of the photonic crystal holes, narrow optical aperture, and large diameter air-holes, we observe that diffraction and mode leakage through the PhC holes becomes the dominating phenomena, and then any fabrication imperfection may contribute to discrepancy between theory and experiment.**

***Index Terms*—Photonic crystal, transverse optical modes, vertical cavity surface emitting lasers (VCSEL).**

I. Introduction

HIGH power, single fundamental mode vertical-cavity surface-emitting lasers (VCSELs) are of great interest for applications such as portable gas sensing, as they provide limited wavelength tunability with injection current and temperature; for telecommunications, data centers and supercomputer optical data interconnects as they are of low cost and high reliability. For those applications, it is desirable to have low-threshold, narrow linewidth light sources which possess high side-mode suppression ratio (SMSR) emission. VCSELs inherently emit in single longitudinal mode; however, lateral mode control is quite demanding. One way of such control is the introduction of photonic-crystal (PhC) to the VCSEL structure, which may ensure single-mode emission in a very broad range of injection currents as shown in [1]–[6]. The mechanism responsible for discrimination of high-order modes originates from two counter-acting phenomena [7].

1) The PhC introduces lateral mode confinement by strong waveguiding effect, i.e., a difference in the effective refractive index of the areas without and with PhC.
2) The PhC holes destroy the vertical periodicity of the VCSEL top distributed Bragg reflectors (DBR) and contribute to a selective reduction of its reflectivity. As a result, the higher-order lateral modes which optical field greatly overlaps the PhC region leak through the holes and become discriminated.

A number of reports have demonstrated the high power, high SMSR operation of PhC VCSEL both experimentally [1]–[6] and theoretically [7]–[9]. There has been an attempt to define a benchmark structure which can serve as a reference for numerical models [10]. The direct comparison between experimental measurements and simulations of single-PhC VCSELs with respect to beam properties and emitted power has been carried out in [11]–[13]. In this paper, we perform extensive, statistical study on agreement between experimental and numerical analysis of emission spectrum of numerous PhC VCSEL configurations. Such analysis is crucial for evaluation of the numerical models used to simulate the complex PhC VCSEL structure, as well as for better understanding of the numerous physical phenomena occurring in these lasers.

In this paper, we present a direct comparison of the experimental emission spectra of 980 nm PhC VCSELs with various PhC parameters and etched hole depths with the simulated resonant wavelengths and the corresponding modal gains. We also perform a statistical analysis of the spectral splitting between the fundamental (HE_{11}) and first-order (HE_{21}) modes which reveals the onset of PhC induced waveguiding.

II. PhC VCSEL Structure and Measurements

Our study is based on 980-nm VCSELs as described in Table I. The current flow is defined by 12-μm diameter aperture, selectively oxidized in the $Al_{0.98}Ga_{0.02}As$ layer in the first period of the top DBR. The active region is composed of three

Manuscript received October 31, 2012; revised December 19, 2012 and January 15, 2013; accepted January 16, 2013. This work was supported in part by Grant COST MP0702, in part by the Swiss National Science Foundation (SNF) under Grant SCOPES IZ73ZO_128019, National Centre of Research and Development "Novel Photonic Crystal Surface Emitting Lasers Incorporating a High-Index-Contrast Grating" and in part by the European Union within European Regional Development Fund, under grant Innovative Economy (POIG.01.03.01−00−159/08, "InTechFun"). M. Dems acknowledges the support of Polish National Center for Research and Development within the project LIDER. The work of K. Panajotov was supported by IAP 6/10 – Belgian Science Policy, FWO Flanders, GOA, and OZR of the Vrije Universiteit Brussel.

T. Czyszanowski, M. Dems, and R. P. Sarzała are with Institute of Physics, Lodz University of Technology, Lodz 90-924, Poland (e-mail: tomasz.czyszanowski@p.lodz.pl; maciej.dems@p.lodz.pl; robert.sarzala@p.lodz.pl).

K. Panajotov is with Department of Applied Physics and Photonics, Vrije Universiteit Brussels, Brussels 1050, Belgium, and also with Institute of Solid State Physics, Sofia 1784, Bulgaria (e-mail: kpanajot@b-phot.org).

K. D. Choquette is with Department of Electrical and Computer Engineering, University of Illinois at Urbana-Champaign, Urbana, IL 61801 USA (e-mail: choquett@illinois.edu).

Color versions of one or more of the figures in this paper are available online at http://ieeexplore.ieee.org.

Digital Object Identifier 10.1109/JSTQE.2013.2247568

TABLE I
LAYER THICKNESSES AND REFRACTIVE INDICES OF 980-nm VCSEL

Alloy	Refractive index	Layer thickness [um]	Repetition
$Al_{0.16}Ga_{0.84}As$	3.418	0.07168	19
$Al_{0.92}Ga_{0.08}As$	2.983	0.08213	19
$Al_{0.16}Ga_{0.84}As$	3.418	0.07168	1
$Al_{0.98}Ga_{0.02}As/Al_xO_y$	2.955/1.75	0.08291	1
$Al_{0.5}Ga_{0.5}As$	3.208	0.11721	1
GaAs	3.527	0.01	3
$In_{0.2}Ga_{0.8}As$	3.62	0.008	3
GaAs	3.527	0.01	1
$Al_{0.5}Ga_{0.5}As$	3.208	0.11721	1
$Al_{0.92}Ga_{0.08}As$	2.983	0.08213	35
$Al_{0.16}Ga_{0.84}As$	3.418	0.07168	35
GaAs	3.527	4	1

8-nm $In_{0.2}Ga_{0.8}As$ quantum wells separated by GaAs barriers. The $Al_{0.5}Ga_{0.5}As$ cavity is bounded by 19 and 35 periods of $Al_{0.16}Ga_{0.84}As/Al_{0.92}Ga_{0.08}As$ DBRs on the top and bottom, respectively. The PhC is etched in the top DBR in the form of a hexagonal lattice of air holes with a central single defect.

The epitaxial layer thickness of the experimentally investigated PhC VCSELs varies within 10 nm resulting in a variation of the VCSEL cavity resonant wavelength in the 30-nm range. In order to avoid fine tuning adjustment of the layers thickness for each PhC VCSEL separately, we fix the thicknesses of all VCSEL layers as given by the design in Table I, and then linearly shift the experimental spectra to assure identical wavelengths of the measured and computed fundamental mode. This procedure is justified as we are interested in the wavelength difference between the fundamental and higher order modes rather than the absolute position of the fundamental mode.

The PhC patterns are defined by optical lithography and etched by inductively coupled plasma-reaction ion etching; the details of device fabrication can be found in [4]–[6]. The PhC hole depths are controlled by the time of etch, and for the samples considered here we use etches of 7 and 9 min. duration. The resulting etching depths are dependent on the hole diameter [4] and are listed in Table II with the experimental dimensions and parameters of the PhCs. The sub-threshold spectra (typically $0.9 \times$ threshold current) are obtained for each device listed in Table II. The continuous wave emission is carefully focused onto a fiber-coupled optical spectrum analyzer.

III. MODEL

The optical, electrical and, thermal models used here are described in detail in [14], [15]. We employ a fully vectorial 3-D optical solver based on the plane wave admittance method [8]. We stress that PhC VCSEL analysis performed by the optical effective model [6] would not resolve the spectral behavior presented here since in this approach the refractive indices of

TABLE II
PHOTONIC-CRYSTAL ETCHING DEPTHS FOR TWO DIFFERENT ETCHING DURATIONS (a –IS THE DISTANCE BETWEEN CENTERS OF THE HOLES, b –IS THE HOLE DIAMETER)

PhC parameters		Etching depths [nm]	
b/a	*a* [μm]	7 minutes etching (no of sample)	9 minutes etching (no of sample)
0.4	3.5	1371 (1)	n/a
0.4	4	1371 (2)	n/a
0.4	4.5	1371 (3)	2906 (4)
0.4	5	1371 (5)	2982 (6)
0.4	5.5	1447 (7)	3021 (8)
0.4	6	1524 (9)	3059 (10)
0.5	4	1371 (11)	3059 (12)
0.5	4.5	1447 (13)	3059 (14)
0.5	5	1524 (15)	3097 (16)
0.5	5.5	1601 (17)	3136 (18)
0.5	6	1678 (19)	n/a
0.6	4	1524 (20)	n/a
0.6	4.5	1563 (21)	n/a
0.6	5	1601 (22)	n/a
0.6	5.5	1601 (23)	n/a
0.6	6	1601 (24)	n/a
0.6	6.5	1639 (25)	n/a
0.6	7	1678 (26)	n/a

particular parts of the device are averaged in longitudinal direction and transformed into uniform blocks defined by constant, effective refractive indices. As a result, the influence of the PhC is manifested in these models by the waveguiding effect only, omitting the PhC induced leakage and scattering optical losses. Using an effective index model requires further matching to experimental parameters, such as subthreshold spectral measurements to extract effective optical loss [6]. Our model used here has previously simulated 1.3-μm QD VCSEL, confirming very good agreement between the model calculations and experiment measurements [16].

IV. COMPARISON OF EXPERIMENTAL AND THEORETICAL SPECTRAL CHARACTERISTICS OF 980-nm PhC VCSELS

To simulate the realistic modal behavior of PhC VCSEL, we first perform thermal and electrical self-consistent calculations for close to threshold operation of the VCSEL without PhC as shown in Fig. 1(a). The main heat source is located in the active region and is generated by the nonradiative recombination processes in the quantum wells and by the Peltier effect at the edges of the active region where the carriers cross 0.6 eV energy step from the $Al_{0.5}Ga_{0.5}As$ cladding to the GaAs barrier. Their additional kinetic energy is dissipated through the phonons contributing to the heating the structure. The heat generated in the active region and its proximity is transferred to the substrate heat sink but some part is accumulated in the top DBR since

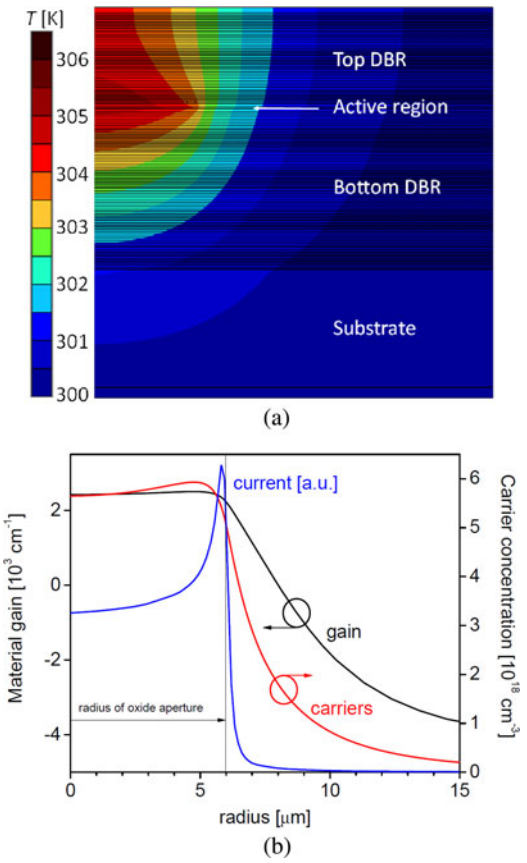

Fig. 1. (a) Calculated temperature distribution in the VCSEL structure as given by the design (see Table I). (b) Profiles of the gain (the black curve, left axis), carrier concentration (the red curve, right axis) and injection current (blue) in the active region.

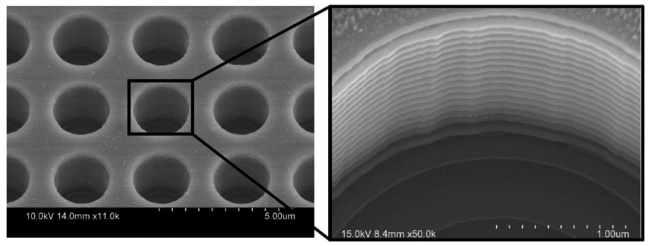

Fig. 2. Scanning electron microscope picture of the PhC hole etched in $Al_{0.16}Ga_{0.84}As$/ $Al_{0.92}Ga_{0.08}As$ DBR. Right panel shows the magnification of the single hole. White contours correspond to the interfaces between the layers. Three bottom contours are of significantly smaller diameter reviling rounding of the hole bottom.

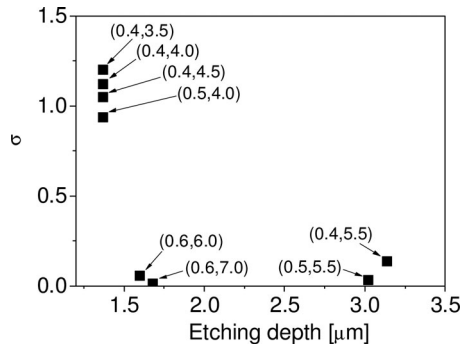

Fig. 3. Relative error σ of wavelength splitting between the HE_{11} and the HE_{21} modes calculated with continuous-wave model and cold-cavity model as a function of the etching depth.

there is no efficient mechanism for thermal dissipation except for heat convection in the air. The temperature increase in the active region with respect to the ambient temperature is only 4 K, which induces a 1.2×10^{-3} change of the refractive index, which is two orders of magnitude smaller than the refractive index change caused by the oxide confinement.

The current distribution reveals strong current crowding effect due to the top ring-shaped contact, as depicted in Fig. 1(b). The high current density at the oxide aperture periphery is not evident as equally severe nonuniform carrier distribution due to the carrier diffusion process, which results in a smoother profile with only a 5% nonuniformity. The gain distribution is also fairly uniform across the device due to the nearly logarithmic dependence of the material gain on the carrier concentration. In our calculations of PhC VCSELs with different PhC parameters, we use similarly calculated temperature and gain distributions as shown in Fig. 1. This simplification makes the calculations efficient, provides thermal focusing, and current crowding effects which can contribute to the competition between the modes, and may affect the spectrum of the laser. To prove that this simplification does not introduce significant error, we calculate the thermal impedance of the VCSEL without a PhC, which equals $Z = 1280$ K W^{-1}. We find that the maximal temperature under the same level of injection and for plethora of different PhC parameters changes the thermal impedance insignificantly. For example, the temperature increase is less than 2% even when the PhC holes extend throughout the whole top DBR, which is the most severe impact of the PhC on the thermal conductivity of the top DBR. Based on these calculations, we find an empirical linear dependence for the impact of the PhC on the thermal impedance: $\Delta Z = b/a\, d_E$ 14 K W^{-1} μm^{-1}, where b is diameter of the air hole, a is the distance between the centers of the holes and d_E is the etching depth given in μm. This formula is valid for $b/a \leq 0.7$.

Although the current is injected through the top DBR, the electrical resistance of the structure changes insignificantly with the change of the etching depth, which we have proven experimentally [17] and numerically [18]. Additionally we have shown that relative variation of the carrier distribution in the active region is less than 5% for the PhC holes with b/a ratio in the range from 0.4 to 0.6 [18].

It is worth mentioning that, in order to better represent the actual etched hole profiles, the bottoms of the PhC holes have been rounded in the calculations, with rounded part extending 3 DBR layers (1.5 period) in length (see Fig. 2). The indicated hole depth is the distance from the top VCSEL facet to the very bottom of the rounded portion of the hole.

First we perform a comparison of the relative error

$$\varepsilon = \frac{\lambda_{\mathrm{H11}}^{\mathrm{cc}} - \lambda_{\mathrm{HE21}}^{\mathrm{cc}}}{\lambda_{\mathrm{H11}}^{\mathrm{cw}} - \lambda_{\mathrm{HE21}}^{\mathrm{cw}}} \tag{1}$$

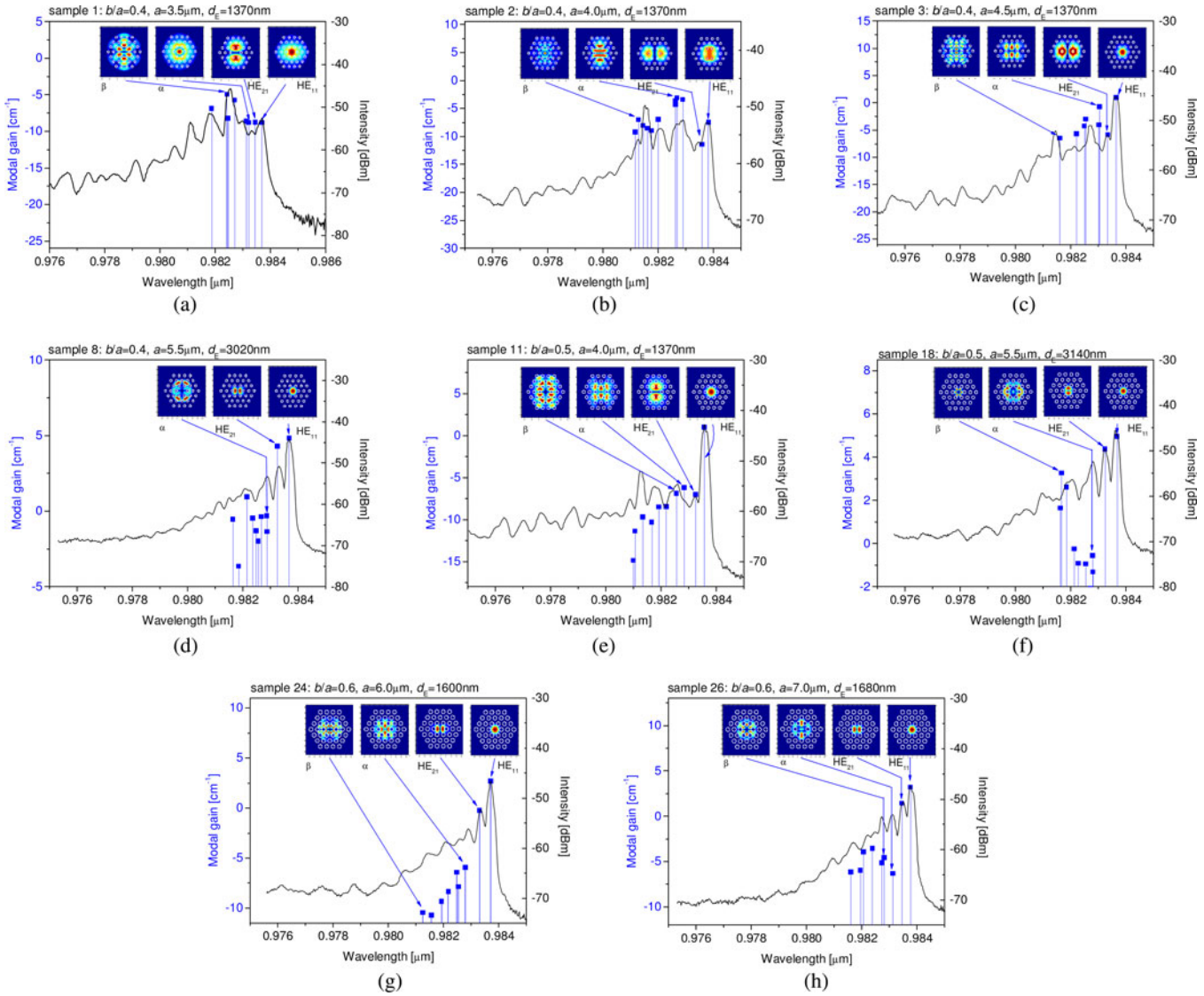

Fig. 4. (a)–(h) Experimental spectra (right vertical axes) and calculated resonant modes (squares with vertical lines and left vertical axes) for PhC VCSEL with different PhC parameters: a—distance between the PhC holes, b— diameter of the holes, d_E — hole etching depth. The insets show the calculated intensity distribution of selected resonant modes in the plane of the active region.

of the wavelength splitting between modes HE_{11} and HE_{21} in cw (continues-wave) operation model, i.e., λ_{11}^{cw} and λ_{21}^{cw} and cold-cavity model, i.e., λ_{11}^{cc} and λ_{21}^{cc} for several arbitrary chosen samples of PhC VCSELs (see Fig. 3). One can notice that ε is drastically reduced for deeper than 1.5 μm etching, which corresponds to strong HE_{21} mode confinement. That effect will be further elaborated with greater details. ε is smaller if the PhC confinement is stronger, which can be realized by deeper holes or/and wider holes with smaller distance between them. In the cold cavity model, HE_{21} modes are dominantly confined by the broad oxide aperture, which contributes to the strong overlap of the HE_{21} modes with the holes. In the common wave (CW) model, the waveguide effect of the PhC is supported by thermal focusing and HE_{21} modes can be more efficiently confined to the PhC aperture. In the further analysis, we perform the calculation with the CW model.

In Fig. 4, we present a comparison of the experimentally measured (and sometimes shifted) subthreshold emission spectra with the computed optical modes and modal gains. For the purpose of detailed comparison with the experimental spectral characteristics, we compute up to 20 consecutive resonant modes starting with the fundamental mode with the longest wavelength. Modes with modal losses larger than 20 cm^{-1} are not taken into account. For each resonant mode, the emission wavelength and modal gain are calculated. If the modal gain is larger than zero, then the mode is lasing under the specific conditions determined by the distribution of the material gain and temperature. The modal gain of a particular mode is proportional to the emitted power of that mode only in proximity of threshold. Above threshold nonlinear effects triggered by the spatial hole burning lead to mode competition and, therefore, the modal gain is not linearly related to the mode intensity.

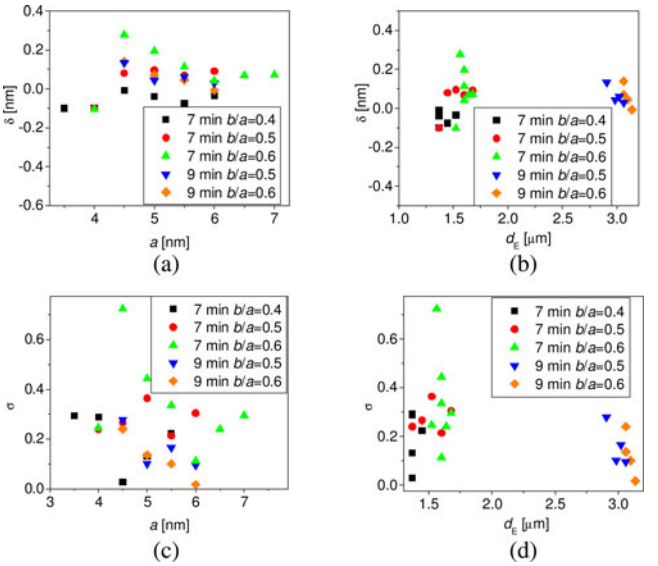

Fig. 5. (a), (b) absolute (δ) and (c), (d) relative (σ) error of calculation of HE_{11} and HE_{21} wavelength splitting as a function of the distance between holes (a), (c) and etching depth (b), (d). Squares, circles, and triangles correspond to 7 min etching and b/a ratios of 0.4, 0.5, and 0.6, respectively. Inverted triangles and inverted squares correspond to 9 min etching and b/a ratios of 0.5 and 0.6, respectively.

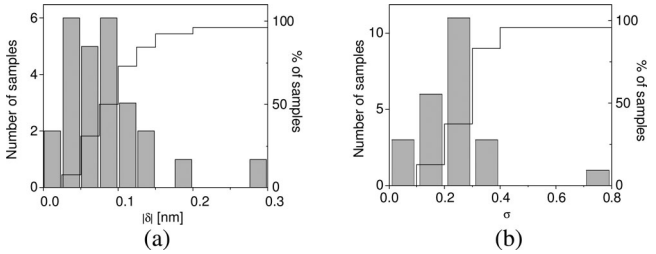

Fig. 6. Histogram of the absolute δ (a) and the relative σ (b) errors. The columns showing the number of samples with error in a specific range are referred to the left axes. The step function determining the percentage of the samples with an error less than a specific value is referred to the right axes.

To simulate correctly those behaviors one needs an aforementioned threshold multitransverse-mode model, which are very time consuming and, therefore, not considered here.

The labeling of the analyzed modes is somewhat complicated since the reflections and diffraction of the PhC holes strongly impacts the mode distribution. The fundamental (HE_{11}) and first order modes (HE_{21}) can be easily recognized, since they are confined by the PhC defect in most of the cases, and since they are the lowest order even and odd modes, respectively. Far more ambiguous is the recognition of higher order modes which are not confined by the PhC, but by the oxide aperture and for this reason, they are labeled by successive Greek letters rather than by the hybrid-modes designation (HE_{ij}).

The optical calculations performed for VCSELs with PhCs defined in Table II show that for samples 1 and 2 [see Fig. 4(a) and (b)] HE_{11} is weakly confined by the photonic crystal. The insets show that the fundamental mode largely overlaps the PhC lattice, and the field that extends to the bottom of the holes leaks from the structure. The fundamental mode distribution far from Gaussian shape [see Fig. 4(b)] is the effect of the strong leakage. The process of the modification of the lateral mode distribution by the PhC is described with details in [9]. The fingerprint of weak PhC confinement is a broad experimental spectrum in which the fundamental mode is of low intensity. In such a case, the modes are dominantly confined by the oxide aperture. The calculated modal gains confirm this conclusion showing that indeed, the fundamental mode exhibits low modal gain. Several other modes, like the one assigned by β and α in the insets of Fig. 4(a) and (b), possess higher modal gains. This results from the fact that the maxima of the optical field distributions of these modes are located between the holes and they do not leak as intense through the holes as the other transverse modes. The PhC lattice with other PhC parameters are able to confine at least the fundamental mode as observed both in the experiment and in the calculations. The samples 7, 18, 24, and 26 characterized by deep hole etching and/or broad-area PhC defect enable PhC confinement of two modes as shown in Fig. 4(d), (f), (g), (h). In our computations, we rarely observe cases for which the third mode is well confined into the PhC defect, such an example is sample 18 shown in Fig. 4(f). In most of the cases, the third mode is weakly confined to the PhC defect, e.g., samples 24, 26 shown in Fig. 4(g), (h). In those cases, the mode is located between the holes of the first PhC ring, which can explain the broad mode distribution and the simultaneously low optical losses.

Fig. 4(a)–(h) shows good correspondence between theory and experiment: either single numerically calculated modes or groups of the modes are located in the proximity of the experimentally measured spectral peaks. Moreover, the theoretical modal gains are consistent with the experimentally measured mode intensities. As mentioned previously, the modal gains can be related to the mode intensities near lasing threshold. The above threshold operation is highly nonlinear process and one should not expect good correlation between experiment and our linear threshold model. However, the presented experimental spectra are taken close to threshold and therefore, the calculated modal gains well represent the dominant modes.

Samples 1 and 2 [see Fig. 4(a) and (b)] correspond to weak PhC guidance and the modes defined by the largest wavelengths are not the dominant ones. Such behavior is confirmed both by the experiment and the theory. On the other extreme, sample 11 reveals single- mode operation which is confirmed by the SMSR close to 10 dB in the experiment and by the theoretical modal gain difference between HE_{11} and HE_{21} modes close to 10 cm^{-1}. Although experimental and theoretical results cannot be directly compared since our model does not take into account above threshold operation, qualitative comparison to other samples nevertheless reveals that sample 11 is superior with respect to higher order modes discrimination both experimentally and theoretically. The fundamental mode is also dominating for other samples both in the experiment and theory but more precise analysis does not show a very good correlation.

Since the experimental spectra are uniformly shifted in order to adjust the experimental to the simulated fundamental mode wavelength to avoid complications from layer thickness uniformity, the most reasonable parameter in a comparative analysis

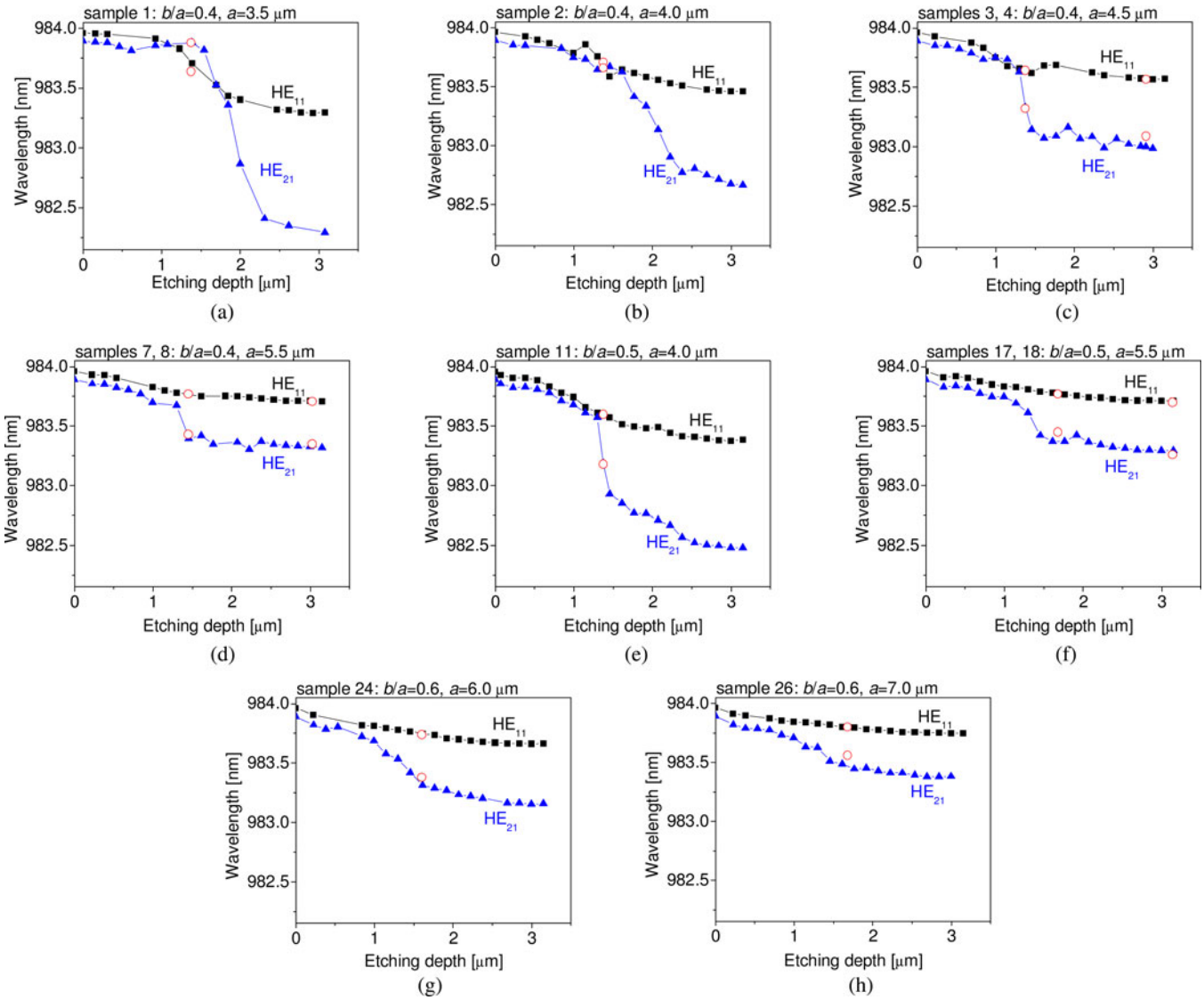

Fig. 7. (a)–(h) Calculated wavelengths of the fundamental (HE_{11} - squares) and the first-order mode (HE_{21}–triangles) as a function of the etching depth and for different diameters of the PhC holes (a) and ratios (b/a). Open circles correspond to the experimental results analyzed in Figs. 4 and 5.

would be the wavelength splitting between the fundamental and the higher order modes. Third- and higher order modes might be strongly suppressed and difficult to unambiguously determine from the experimental spectra. Hence, the wavelength splitting between the two lowest order modes (HE_{11} and HE_{21}) would be the best parameter choice for comparison.

We define the parameters δ and σ as the absolute and relative errors, respectively in the wavelength difference between HE_{11}, HE_{21}

$$\delta = \left(\lambda_{\mathrm{H11}}^{\mathrm{Exp}} - \lambda_{\mathrm{HE21}}^{\mathrm{Exp}}\right) - \left(\lambda_{\mathrm{H11}}^{\mathrm{Calc}} - \lambda_{\mathrm{HE21}}^{\mathrm{Calc}}\right) \tag{2}$$

$$\sigma = \left| \frac{\delta}{\lambda_{\mathrm{H11}}^{\mathrm{Exp}} - \lambda_{\mathrm{HE21}}^{\mathrm{Exp}}} \right| \tag{3}$$

where λ^{Exp} and λ^{Calc} are the wavelengths determined in experiment and in calculations, respectively.

Fig. 5 provides a systematic analysis of the parameters δ and σ determined from the experiment and from the calculations. One can notice from Fig. 5 that both errors are larger for smaller a, larger b/a, and shallower etching. Those are the cases for which the resonant modes might be leaking and strong diffraction might occur, since the optical aperture is narrow and the holes have relatively large diameter. In such cases, the interaction of the modes with the air-holes is very intense, and any technological imperfections might have significant impact on the deviation of the results from the ones of perfect holes assumed in the calculation. Any possible systematic error due to our numerical approach has been shown to be less than 0.01 nm [19]. The largest observed absolute (relative) error is 0.3 nm (0.72) for sample 21. Fig. 6 shows the number of samples attributed to the specific absolute and relative errors. It shows that the mean absolute error is close to 0.07 nm and that 90% of samples are attributed to δ smaller than 0.15 nm.

The mean relative error is close to 0.2 and more than 95% of samples are attributed to σ smaller than 0.4.

The second part of our analysis is presented in Fig. 7 which depicts the calculated wavelengths of the fundamental (HE_{11}) and the first order mode (HE_{21}) as a function of the etching depth together with the experimental results (open circles). One can observe that an increase of the etching depth contributes to a blue-shift in wavelength, and to an increase of the wavelength splitting $\Delta\lambda$ between the HE_{11} and the HE_{21} modes, both of which are consistent with increased index confinement. For shallow etching, the PhC defect is not acting as confinement mechanism. The modes are confined by the broad oxide aperture and their wavelengths are very close to each other. With increasing etching depth the PhC index confinement increases, resulting in the blue-shift of the HE_{21} mode and in a significant wavelength splitting $\Delta\lambda$.

This change of the mode confinement mechanism can be an abrupt process triggered by a small change of the etching depth. Once the etching depth is sufficient for the PhC to confine a mode, further increase in the hole depth does not significantly change either its resonant wavelength or its transverse distribution. Most VCSELs with shallow etching (7 min) are close to the transition point from un-confined by the PhC to well-confined HE_{21} mode. This is the additional reason for the larger error of "7 min" samples discussed previously. Small inaccuracy of the determination of the etching depth of the PhC VCSEL can contribute to a significant error in that range of etching depths. Some small oscillations of the wavelength with increasing etching depth (especially for the HE_{21} mode) are observed in Fig. 7 and originate from the oscillatory behavior described in [9]. The rounding of the PhC hole bottoms reduces the amplitude of these oscillations with respect to the case of flat holes; however, it does not remove them completely.

It is important to note that a critical hole depth that creates the onset the PhC index confinement of the fundamental mode is clearly observed in the simulations. This depth varies around 1.5 μm depending on the PhC parameters, which is in a good agreement with [20]. The fingerprint of the fundamental mode confinement is the appearance of relatively large spectral splitting between the fundamental and the first-order mode.

V. Conclusion

We have presented a detailed comparison of experimental and simulated optical spectra of 980-nm PhC VCSELs. The simulations are based on fully vectorial, 3-D optical model (plane wave admittance method) combined with electrical and thermal finite-element models. We demonstrate good qualitative agreement of the experimental spectra with the calculated emitted wavelengths, thus validating our numerical approach. Although the theoretical model does not account for spatial hole burning effect, we find that a modal gain analysis valid near lasing threshold provides consistent agreement with the experiment information about the dominant transverse modes of PhC VCSELs over a broad range of PhC parameters. Our statistical analysis shows that the strong confinement introduced by the PhC contributes to the conformity between experiment and theory. In a range of PhC parameters where diffraction and mode leakage through the PhC holes dominate, our numerical results show larger deviation from the experiment, e.g., for shallow etching, narrow optical aperture, and broad air holes any technological imperfection may contribute to discrepancy between theory and experiment. The analysis reported here indicates that the mean relative error of the spectral distance between HE_{11} and HE_{21} modes is close to 0.07 nm and that more than 90% of samples fall in an error range less than 0.15 nm.

References

[1] H. J. Unold, M. Golling, R. Michalzik, D. Supper, and K. J. Ebeling, "Photonic crystal surface-emitting lasers: Tailoring waveguide for single-mode emission," in *Proc. 27th Eur. Conf. Optical Commun.*, 2001, pp. 520–521.

[2] D. S. Song, S. H. Kim, H. G. Park, C. K. Kim, and Y. H. Lee, "Single-fundamental-mode photonic-crystal vertical-cavity surface-emitting lasers," *Appl. Phys. Lett.*, vol. 80, pp. 3901–3903, 2002.

[3] N. Yokouchi, A. J. Danner, and K. D. Choquette, "Two-dimensional photonic crystal confined vertical-cavity surface-emitting lasers," *IEEE J. Sel. Topics Quantum Electron.*, vol. 9, no. 5, pp. 1439–1445, Sep./Oct. 2003.

[4] A. M. Kasten, M. P. Tan, J. D. Sulkin, P. O. Leisher, and K. D. Choquette, "Photonic crystal vertical cavity lasers with wavelength independent single mode behavior," *IEEE Photon. Tech. Lett.*, vol. 20, no. 23, pp. 2010–2012, Dec. 2008.

[5] D. F. Siriani, M. P. Tan, A. M. Kasten, A. C. Lehman Harren, P. O. Leisher, J. D. Sulkin, J. J. RafteryJr., A. J. Danner, A. V. Giannopoulos, and K. D. Choquette, "Mode control in photonic crystal vertical-cavity surface-emitting lasers and coherent arrays," *IEEE J. Sel. Topics Quantum Electron.*, vol. 15, no. 3, pp. 909–917, May/Jun. 2009.

[6] D. F. Siriani, P. O. Leisher, and K. D. Choquette, "Loss-induced confinement in photonic crystal vertical-cavity surface-emitting lasers" photonic-crystal-patterned vertical-cavity surface-emitting laser structures," *IEEE. J. Quantum Electron.*, vol. 45, no. 7, pp. 762–768, Jul. 2009.

[7] T. Czyszanowski, R. P. Sarzała, M. Dems, H. Thienpont, W. Nakwaski, and K. Panajotov, "Strong modes discrimination and low threshold in cw regime of 1300 nm AlInGaAs/InP VCSEL induced by photonic crystal," *Phys. Status Solidi A*, vol. 206, pp. 1396–1403, 2009.

[8] T. Czyszanowski, R. P. Sarzała, M. Dems, W. Nakwaski, and K. Panajotov, "Optimal photonic-crystal parameters assuring single-mode operation of 1300 nm AlInGaAs vertical-cavity surface-emitting laser," *J. Appl. Phys.*, vol. 105, pp. 093102-1–093102-10, 2009.

[9] T. Czyszanowski, M. Dems, R. P. Sarzała, W. Nakwaski, and K. Panajotov, "Precise lateral mode control in photonic crystal vertical-cavity surface-emitting lasers," *IEEE. J. Quantum Electron.*, vol. 47, no. 10, pp. 1291–1296, Oct. 2011.

[10] M. Dems, I.-S. Chung, P. Nyakas, S. Bischoff, and K. Panajotov, "Numerical methods for modeling photonic-crystal VCSELs," *Opt. Expr.*, vol. 18, pp. 16042–16054, 2010.

[11] M. S. Alias and S. Shaari, "Loss analysis of high order modes in photonic crystal vertical-cavity surface-emitting lasers," *IEEE J. Lightw. Technol.*, vol. 28, no. 10, pp. 1556–1563, May 2010.

[12] A. Liu, M. Xing, H. Qu, W. Chen, W. Zhou, and W. Zheng, "Reduced divergence angle of photonic crystal vertical-cavity surface-emitting laser," *Appl. Phys. Lett.*, vol. 94, pp. 191105-1–191105-3, 2009.

[13] P. S. Ivanov, P. J. Heard, M. J. Cryan, and J. M. Rorison, "Comparative study of mode control in vertical-cavity surface-emitting lasers with photonic crystal and micropillar etching," *IEEE J. Quant. Electron.*, vol. 47, no. 9, pp. 1257–1265, Sep. 2011.

[14] M. Dems, R. Kotynski, and K. Panajotov, "Plane wave admittance method—Anovel approach for determining the electromagnetic modes in photonic structures," *Opt. Expr.*, vol. 13, pp. 3196–3207, 2005.

[15] R. P. Sarzała and W. Nakwaski, "Optimisation of the 1.3-μm GaAs-based oxide-confined (GaIn)(NAs) vertical-cavity surface-emitting lasers for their low-threshold room-temperature operation," *J. Phys: Condens. Matter*, vol. 16, pp. S3121–S3140, 2004.

[16] D. Xu, C. Tong, S. F. Yoon, W. Fan, D. H. Zhang, M. Wasiak, Ł. Piskorski, K. Gutowski, R. P. Sarzała, and W. Nakwaski, "Room-temperature continuous-wave operation of the In(Ga)As/GaAs quantum-dot VCSELs for the 1.3 μm optical-fibre communication," *Semicond. Sci. Technol.*, vol. 24, pp. 055003-1–055003-5, 2009.

[17] C. Chen, P. O. Leisher, D. M. Kuchta, and K. D. Choquette, "High-speed modulation of index-guided implant-confined vertical-cavity surface-emitting lasers," *IEEE J. Sel. Top. Quantum Electron.*, vol. 15, no. 3, pp. 673–678, May/Jun. 2009.
[18] T. Czyszanowski, R. P. Sarzała, . Piskorski, M. Dems, M. Wasiak, W. Nakwaski, and K. Panajotov, "Comparison of usability of oxide apertures and photonic crystals used to create radial optical confinements in 650-nm GaInP VCSELs," *IEEE. J. Quantum Electron.*, vol. 43, no. 11, pp. 1041–1047, Nov. 2007.
[19] T. Czyszanowski, M. Dems, H. Thienpont, and K. Panajotov, "Optimal radii of photonic crystal holes within DBR mirrors in long wavelength VCSEL," *Opt. Expr.*, vol. 15, pp. 1301–1306, 2007.
[20] P. Ivanov, Y.-L. D. Ho, M. J. Cryan, and J. Rorison, "Modelling investigations of DBRs and cavities with photonic crystal holes for application in VCSELs," *J. Opt.*, vol. 14, pp. 125103-1–125103-10, 2012.

Tomasz Czyszanowski received the M.Sc. and Ph.D. degrees in physics from the Lodz University of Technology, Lodz, Poland, in 2000 and 2004, respectively and D.Sc. degree in physics from Wroclaw University of Technology, Wrocław, Poland, in 2012. His Ph.D. work was involved in the field of determination of validity limits of approaches to optical fields in diode lasers.

After receiving the M.Sc. he was a Visiting Researcher in CFD Research Corporation, Huntsville, AL, USA, where he worked mainly on optical scalar models of semiconductor lasers. From 2005 to 2007, he was a Postdoctoral Researcher at Vrije University, Brussels, Belgium as a fellow of Foreign Fellowships for Young Ph.D.'s awarded by Foundation for Polish Science. There he analyzed the photonic-crystal VCSELs performance. In 2012, he was appointed an Associate Professor in the Institute of Physics at Lodz University of Technology. He authored or co-authored more than 40 publications more than 40 publications in international conference proceedings and 2 book chapters. His research interest includes modeling and designing of the VCSEL arrays and VECSELs.

Maciej Dems received the M.Sc. degree in physics from the Technical University of Lodz, Lodz, Poland, in 2002 in the subject of a strain determination in thin-layered structures, where he is currently working toward the Ph. D. degree

He has participated three times in the short-term scientific missions to the Department of Applied Physics and Photonics, Vrije University, Brussels, Belgium, where he worked on the numerical simulation of optical properties of photonic crystals. His research interests include photonic bandgap materials and their application to the new-generation light-emitting instruments.

Mr. Dems is a regular member of the Optical Society of America.

Robert P. Sarzała received the M.Sc. degree in technical physics from the Technical University of Lodz, Lodz, Poland, in 1989, the Ph.D. degree in electrical engineering from the Institute of Electron Technology, Warsaw, Poland, in 1998, and the D.Sc. degree in physics from the Institute of Physics, Wrocław University of Technology, Wrocław, in 2006.

In 1990, he joined the Laboratory of Computer Physics, Institute of Physics and the teaching staff of the Faculty of Technical Physics, Computer Science and Applied Mathematics, both at the Technical University of Lodz. In 2007, he became an Associate Professor at the Institute of Physics, with teaching responsibilities in photonics. His research interests include self-consistent computer modeling of physical phenomena crucial for operation of diode lasers. In particular, he is interested in simulation of optical, electrical, thermal, and mechanical phenomena taking place during operation of in-plane diode lasers and vertical-cavity surface-emitting diode lasers as well as of diode-laser arrays. Recently, he has been involved in an intense investigation of laser devices which may be used in modern optical-fiber communication systems taking advantage of successive "optical windows" (0.85 μm, 1.3 μm, and 1.55 μm). In particular, he is involved in the field of modeling of the operation of GaAs-based diode lasers with both the (GaIn)(NAs)/GaAs quantum-well and the InAs/GaAs quantum-dot active regions.

Krassimir Panajotov received the B.S., Ph.D., and D.Sc. degrees in physics from Sofia University, Sofia, Bulgaria, in 1982, 1988, and 2002, respectively.

Since 1982, he has been at the Institute of Solid-State Physics (ISSP), Bulgarian Academy of Sciences, Sofia, Bulgaria. Since 2001, he has been leading the group on micro- and nano Photonics at ISSP. During 1996–1998, he was a Guest Researcher at the Vrije Universiteit Brussels, Brussels, Belgium, which he joined again in 2000. His research activities are in nonlinear optics, semiconductor lasers, photonic crystal devices, and nonlinear semiconductor laser dynamics. In these fields, he holds more than 140 SCI-stated journal papers, more than 150 publications in international conference proceedings and 3 book chapters.

Dr. Panajotov has led a number of projects on national level in Bulgaria and Belgium and international bilateral projects and served as a national coordinator of several European COST actions. He Cochaired the conferences on Semiconductor Laser and Laser Dynamics at the Photonics Europe'2008, '2010 and '2012 and five International Workshops. He has served as a Guest Editor of four Special Issues: three of journal of *Optical and Quantum Electronics* and one of journal of *Advances in Optics Technologies*, as well as of three SPIE proceedings. He is currently an Associate Editor of the *Journal of Opto-Electronics Review* on the topic of Photonic Crystals. He is a a Senior member of OSA.

Kent D. Choquette (M'97–F'03) received the B.S. degree in engineering physics and applied mathematics from the University of Colorado, Boulder, USA, and the M.S. and Ph.D. degrees in materials science from the University of Wisconsin-Madison, Madison, USA.

He was with Sandia National Laboratories, Albuquerque, NM, USA, after a Postdoctoral appointment at AT&T Bell Laboratories, Murray Hill, NJ, USA. Since 2000, he has been a Professor in the Department of Electrical and Computer Engineering, University of Illinois at Urbana-Champaign, Urbana, USA. He has authored more than 200 publications and three book chapters, and has presented numerous invited talks and tutorials. His current research interests include the design, fabrication, characterization, and applications of vertical-cavity surface-emitting lasers, photonic crystal light sources, nanofabrication technologies, and hybrid integration techniques for photonic devices.

Dr. Choquette is a Fellow of the Optical Society of America and the Society of Photo-Optical Instrumentation Engineers. He was awarded the 2008 IEEE/Lasers and Electro-Optical Society Engineering Achievement Award. He has served as an Associate Editor of the IEEE JOURNAL OF QUANTUM ELECTRONICS, IEEE PHOTONIC TECHNOLOGY LETTERS, and *Journal of Lightwave Technology*, as well as a Guest Editor of the IEEE JOURNAL OF SELECTED TOPICS IN QUANTUM ELECTRONICS.